Numerical research on mid-infrared supercontinuum generation in $Ge_{11.5}As_{24}Se_{64.5}$ few-mode photonic crystal fibers[*]

SHI Weihua[**], **ZHANG Tiantian**, and **XU Chuanxiang**

College of Electronic and Optical Engineering & College of Flexible Electronics (Future Technology), Nanjing University of Posts and Telecommunications, Nanjing 210023, China

Based on the nonlinear and mode coupling effect in few-mode photonic crystal fiber (FM-PCF), an approach for supercontinuum (SC) generation in the mid-infrared (MIR) region is proposed. The propagation characteristics of $Ge_{11.5}As_{24}Se_{64.5}$ FM-PCF have been analyzed and optimized by the full-vector finite element method. The two-mode generalized nonlinear Schrodinger equation (TM-GNLSE) is set up, and the SC generation has been analyzed by the split-step Fourier method. The SC from 1.80 μm to 11.32 μm is generated by pumping 3.0-cm-long fiber at the central wavelength of 3.0 μm, the peak power of 120 W, and the pulse duration of 250 fs.

The research of mid-infrared (MIR) supercontinuum (SC) has attracted intense attention due to its wide range of applications, such as optical coherence tomography, spectroscopic analysis, fluorescence microscopy and etc[1]. In recent years, a lot of studies of MIR SC generation based on nonlinear effects of optical fibers have been proposed[2-4]. SAINI et al[5] obtained MIR SC spectrum covering the wavelength range from 2.0 μm to 15.0 μm by pumping a triangular-core graded-index single-mode (SM) photonic crystal fiber (PCF) with 3.5 kW laser pulses at 4.1 μm. CHENG et al[6] experimentally demonstrated that MIR SC spanning from 2.0 μm to 15.1 μm can be generated by pumping a 3.0-cm-long step-index single-mode fiber (SMF) with 2.98 MW laser pulses at 9.8 μm. WU et al[7] designed SMF with a suspended-core structure in which SC spectrum from 1.7 μm to 11.3 μm was generated. Although the SC generated by SMF (whether PCF or not) can reach the MIR region, it is still demanding the high pump power, such as few kilowatts[5-11], tens of kilowatts[3,12], and even several megawatts of peak power[6].

On the other hand, the base material of the optical fiber is also an important factor that affects SC generation. To generate MIR SC, several non-silica glasses are preferred, including tellurite[7], fluoride[13] and chalcogenide glasses[2,3,5,6], because these materials possess both wide MIR transparency and relatively high third-order optical nonlinearity. The third-order optical nonlinearity coefficient plays a significant role in the propagation of the pulse through the optical fiber when the wavelength of the input pulse is near the zero dispersion wavelength (ZDW) of the fiber[14].

In this paper, we presented a new approach for generating MIR SC spectra via the mode coupling effect in a few-mode photonic crystal fiber (FM-PCF). First, we designed a chalcogenide glass $Ge_{11.5}As_{24}Se_{64.5}$ FM-PCF with high nonlinearity, flat dispersion, and three ZDWs. Second, we set up the two-mode generalized nonlinear Schrodinger equation (TM-GNLSE) and applied it to the dynamics of SC generation in FM-PCF. The SC generation was investigated via changing the peak power and central wavelength of the pump pulse. When pumping a 3.0-cm-long fiber at the central wavelength of 3.0 μm, the peak power of 120 W, the pulse duration of 250 fs, a SC spectrum from 1.80 μm to 11.32 μm was obtained.

A chalcogenide glass $Ge_{11.5}As_{24}Se_{64.5}$ FM-PCF was designed as shown in Fig.1(a), six smaller air holes with diameter d_2 were added to the first layer in the cladding layer of the PCF, which can reduce the loss of the first-order mode and increase the loss of the high-order mode in the FM-PCF. The air hole diameter is d_1=3 μm, air hole spacing is $\Lambda=d_1/0.55$, $d_2=d_1/2$, and cladding layer number is N=3. The material of the fiber is chalcogenide glass $Ge_{11.5}As_{24}Se_{64.5}$, which has broad transparency in the MIR[15] and its material absorption can be neglected. Furthermore, $Ge_{11.5}As_{24}Se_{64.5}$ has high nonlinear refractive index, which is two orders of magnitude higher than that of silica[15].

Fig.1(b) shows the mode field distributions of HE_{11b}, HE_{11a}, TE_{01}, HE_{21b}, HE_{21a}, and TM_{01}, respectively. The

annular mode TM_{01} is radially polarized, TE_{01} is azimuthally polarized, while HE_{11} and HE_{21} are hybrid polarization modes.
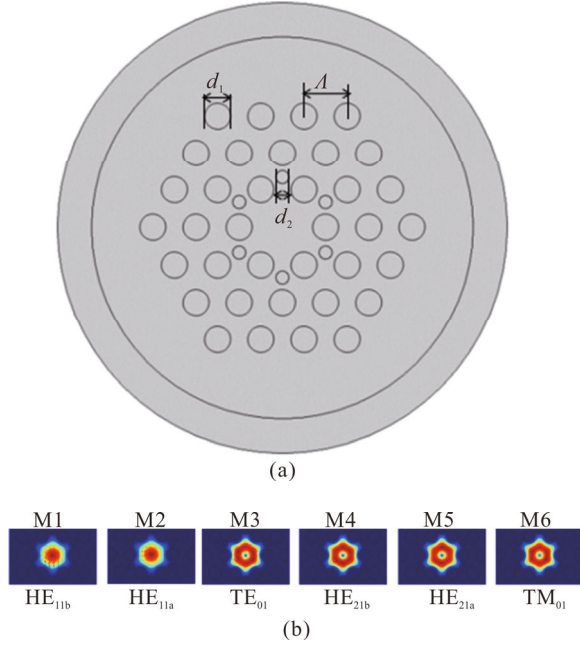

(a)

(b)

Fig.1 (a) Cross section of the proposed FM-PCF; (b) Mode field distributions of the six lowest modes

Fig.2(a) shows the confinement loss curves near 3.0 μm. The confinement loss of each mode increases with wavelength and reaches 10^0 dB/km at 3.0 μm. The confinement loss of HE_{11} is the lowest, then TE_{01}, HE_{21}, and the confinement loss of TM_{01} is the highest relatively.

Fig.2(b) shows the curves of group velocity dispersion (GVD) of the six modes. It can be found that the dispersion characteristics of the six modes are similar and keeping flat dispersion from 2.5 μm to 6.0 μm and there are three ZDMs at 3.0 μm, 4.5 μm, and 6.0 μm. The ZDW plays a critical role in determining the phase-matching conditions and the conversion efficiency in nonlinear parametric processes[16]. Thus, we get a FM-PCF with high nonlinearity, low loss, flat dispersion, and three ZDWs.
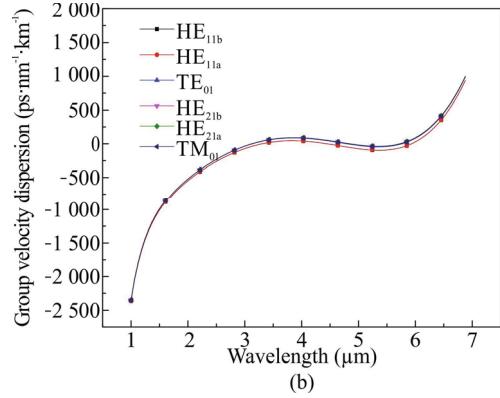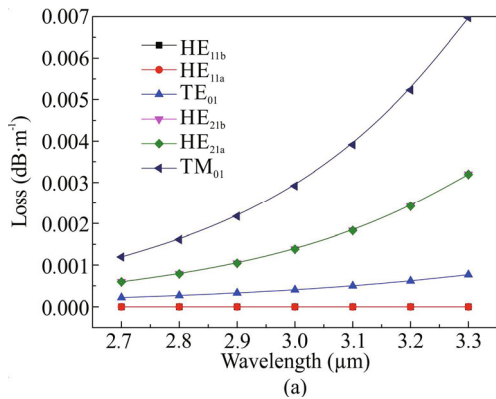

(a)

(b)

Fig.2 Transmission characteristics of six modes in the FM-PCF: (a) Confinement loss curves; (b) Group velocity dispersion curves

The sixth-order Taylor expansion coefficients of the six modes at 3.0 μm are listed in Tab.1. The coefficients of the six modes are numerically similar due to their similar dispersion properties. In particular, the coefficients of HE_{11a} and HE_{11b}, HE_{21a} and HE_{21b} are equal.

Tab.1 Dispersion coefficients of the six lowest modes at 3.0 μm

	HE_{11b}	HE_{11a}	TE_{01}	HE_{21b}	HE_{21a}	TM_{01}
β_1 (s^1/m) ($\times 10^{-9}$)	8.83	8.83	8.88	8.89	8.89	8.89
β_2 (s^2/m) ($\times 10^{-26}$)	2.09	2.09	4.55	3.01	3.01	2.84
β_3 (s^3/m) ($\times 10^{-40}$)	5.59	5.59	9.18	9.65	9.65	9.66
β_4 (s^4/m) ($\times 10^{-54}$)	−5.40	−5.40	−1.24	−1.36	−1.37	−1.35
β_5 (s^5/m) ($\times 10^{-69}$)	1.08	1.08	2.38	2.68	2.68	2.59
β_6 (s^6/m) ($\times 10^{-84}$)	1.71	1.74	3.91	−4.55	−4.55	−4.28

The multiple-mode generalized nonlinear Schrodinger equation (MM-GNLSE) has been adopted for numerically describing ultrashort pulse propagation when multiple transverse modes are excited in an optical fiber[17].

$$\frac{\partial A_p(z,t)}{\partial z} = i(\beta_0^{(p)} - \beta_0) A_p(z,t) - (\beta_1^{(p)} - \beta_1) \frac{\partial A_p(z,t)}{\partial t} +$$

$$i \sum_{n\geq2}^{\infty} \frac{\beta_n^{(p)}}{n!} (i\frac{\partial}{\partial t})^n A_p(z,t) +$$

$$i \frac{n_2 \omega_0}{c} \{ \left(1 + i\tau_{pl}^{(1)} \frac{\partial}{\partial t}\right) \times \left(Q_{pppp}^{(1)} + Q_{plpl}^{(1)} + Q_{ppll}^{(1)} + Q_{pllp}^{(1)}\right) \times$$

$$2 \times A_l(z,t) \int R(t') A_m(z,t-t') \times$$

$$A_m^*(z,t-t') dt' + \left(1 + i\tau_{pl}^{(2)} \frac{\partial}{\partial t}\right) \times$$

$$\left(Q_{pppp}^{(2)} + Q_{plpl}^{(2)} + Q_{ppll}^{(2)} + Q_{pllp}^{(2)}\right) \times 2 \times$$

$$A_i^*(z,t)\cdot\int R(t')A_m(z,t-t')\times$$

$$A_m(z,t-t')\mathrm{e}^{2i\omega_0 t'}\mathrm{d}t'\}=D^{(p)}(z,t)+N^{(p)}(z,t). \quad (1)$$

To simplify the calculations in the PCF where only the fundamental and first-order modes (such as HE_{11b} and HE_{21b} modes) occur, the TM-GNLSE, which consists of a set of equations that are equal to the number of modes, is built instead of MM-GNLSE. Selecting one of the modes (p), the evolution of the pulse envelope $A_p(z, t)$ along the z-axis is described in the co-moving temporal frame as Eq.(1).

Moreover, the nonlinear part $N^{(p)}(z, t)$ includes the mode-coupling part, and Q_{pppp}, Q_{ppll}, Q_{plpl} and Q_{pllp} represent the coupling coefficients between the modes p and l. These coupling coefficients are defined by[17]

$$Q_{plmn}^{(1)}(\omega)=\frac{\iint\left[E_p^*(\omega)\cdot E_l\right]\left[E_m(\omega)\cdot E_n^*(\omega)\right]\mathrm{d}S}{N_p(\omega)N_l(\omega)N_m(\omega)N_n(\omega)},$$

$$Q_{plmn}^{(2)}(\omega)=\frac{\iint\left[E_p^*(\omega)\cdot E_l^*(\omega)\right]\left[E_m(\omega)\cdot E_n(\omega)\right]\mathrm{d}S}{N_p(\omega)N_l(\omega)N_m(\omega)N_n(\omega)},$$

$$(2)$$

where the normalization coefficients are

$$N_p(\omega)=\sqrt{\iint E_p^*(\omega)\cdot E_p(\omega)\mathrm{d}S}, \quad (3)$$

where E_p represents the transverse electric field. The terms $Q_{pppp}^{(1)}$ and $Q_{pppp}^{(2)}$ control the self-phase modulation (SPM), while $Q_{ppll}^{(1)}$ and $Q_{ppll}^{(2)}$ rule the cross-phase modulation (XPM), and the remaining terms $Q_{plpl}^{(1,2)}$ and $Q_{pllp}^{(1,2)}$ enable the four wave mixing (FWM). The effects of XPM and FWM are responsible for the energy transfer between modes, so they occupy a significant proportion of the process of SC generation. It is worth noting that the coefficient $Q_{plmn}^{(1,2)}$ can be expressed in terms of the effective area of the nonlinear interaction between the combination of modes, and $A_{\mathrm{eff},plmn}$ is defined by

$$A_{\mathrm{eff},plmn}=1/(Q_{plmn}^{(1)}+Q_{plmn}^{(2)}). \quad (4)$$

Fig.3 shows how to realize MIR SC generation in the highly nonlinear FM-PCF. The light of a multimode femtosecond laser is incident on a polarization filter composed of a 1D photonic crystal. The TE_{01} and TM_{01} modes are filtered out by the polarization filter at a specific angle[18]. Then the HE_{11a} and HE_{21a} modes are filtered out by popular polarization controller, thus the remaining HE_{11b} and HE_{21b} modes could be focused into the FM-PCF by lens. Finally, the FM-PCF is connected to the optical spectrum analyzer.

In the following, the MIR SC generation processes are simulated based on TM-GNLSE by the split-step Fourier method. To optimize the SC, we first analyzed the influence of fiber length and pulse duration on SC. After continuous optimization, the optimal fiber length is 3.0 cm and the pulse duration is 250 fs. Then the influence of

peak power and center wavelength of pump pulse on SC was analyzed, when the coupling effect between HE_{11b} and HE_{21b} has been considered.
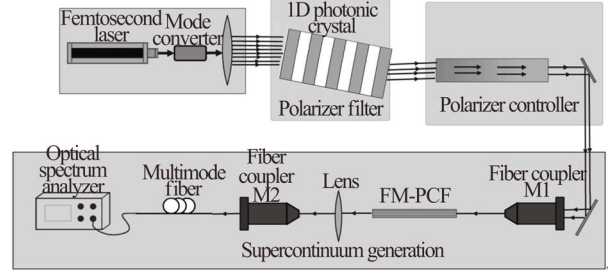

Fig.3 SC generated system diagram in FM-PCF

Fig.4 shows the influence of the peak power of the pump pulse on the SC, where the peak powers are 80 W, 100 W, 120 W, and 140 W when pumping a 3.0-cm-long fiber at the central wavelength of 3.0 µm and the pulse duration of 250 fs. The higher the peak power of the pulse, the wider the range of SC generation, and the range of the spectrum can extend from 1.80 µm to 17.80 µm in the FM-PCF. However, in the long wavelength region, the spectrum oscillates sparsely, and when the peak power increases to 140 W, the flatness of the spectrum gradually decreases.
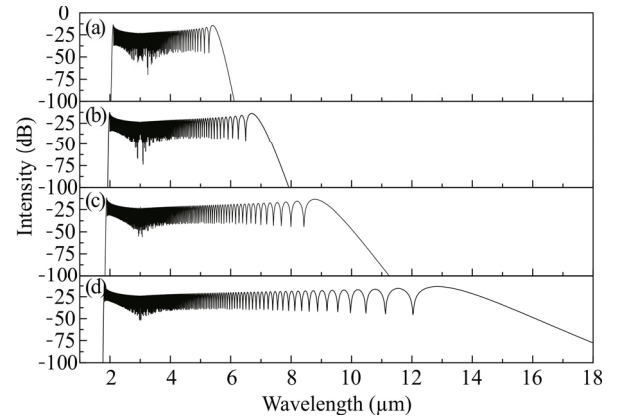

Fig.4 Simulated SC evolution with different peak powers of the pump pulse when pumping a 3.0-cm-long fiber at the central wavelength of 3.0 µm with the pulse duration of 250 fs: (a) *P*=80 W; (b) *P*=100 W; (c) *P*=120 W; (d) *P*=140 W

SPM extends the initial spectrum to either end of the central wavelength, whereas XPM and FWM are the main factors for asymmetrical spectral distribution. When the peak power of the pulse is small, SPM plays a dominant role, and the generated SC is symmetrical relatively. When the pump power is large, XPM and FWM could produce the new frequency components in the MIR to broaden the SC spectrum further, and the generated SC is asymmetrical relatively.

Tab.2 shows the effect of the central wavelength of the pump pulse on the SC when pumping a 3.0-cm-long fiber

at the peak power of 120 W and the pulse duration of 250 fs. As shown in Tab.2, when λ_0=4.5 μm, the SC spectrum expands from 3.30 μm to 6.35 μm. The blue shifted component was almost equal to the red shifted component, i.e., the two components are transmitted equally. This effect results in an almost symmetrically distributed SC spectrum. When λ_0=3.0 μm, the SC spectrum ranged from 1.80 μm to 11.32 μm, with an expansion of 9.52 μm. The blue shifted component was much smaller than the red shifted component, i.e., the blue shifted component is transmitted much slower than the red shifted component. Thus, the SC spectral distribution was asymmetric towards the infrared region.

Tab.2 Influence of the central wavelength of the pump pulse on the SC

Center wavelength (μm)	Shortest wavelength point (μm)	Longest wavelength point (μm)	Spectral range (μm)
3.0	1.80	11.32	9.52
4.5	3.30	6.35	3.05
6.0	3.70	12.50	8.80

Finally, when λ_0=6.0 μm, the SC spectrum ranged from 3.70 μm to 12.50 μm, with an expansion of 8.80 μm. The blue shifted component was smaller than the red shifted component, and as before, the SC spectral distribution is still asymmetric towards the infrared region. Therefore, the SC spectrum pumped at λ_0=3.0 μm is wider and covering MIR bands. In addition, the femtosecond pulse source of the central wavelength at 3 μm is more easily obtained.

Performance comparison of MIR SC proposed with the results of existing literature has been shown in Tab.3. It can be seen that MIR SC generated in the paper can take both lower pump power and wider spectral range into account.

Tab.3 Performance comparison of MIR SC with the existing references

Reference	Fiber structure	Pump power	Spectral range (μm)
[2]	SM-PCF	350 W	1.6—4.2
[3]	SMF	50 kW	0.59—5.52
[4]	PCF+HNLF	150 W	0.5—3.0
[5]	SM-PCF	3.5 kW	2.0—15.0
[8]	SM-PCF	1 kW	2.6—6.857
[9]	FM-PCF	4.8 kW	2.6—6.0
[11]	FM-PCF	30 kW	2.0—14.0
This work	FM-PCF	120 W	1.80—11.32

In this article, a method for generating MIR SC spectra based on the mode coupling effect in FM-PCF has been proposed. A new type of FM-PCF is designed with high nonlinearity, flat dispersion, and three ZDWs. The fiber structure parameters are optimized and the propagation characteristics of the FM-PCF have been analyzed by the full-vector finite element method. The TM-GNLSE is set up and applied to discuss the dynamics of SC generation in the FM-PCF where only the fundamental and first-order modes (HE_{11b} and HE_{21b}) are considered.

From the numerical analyses of the pump power and central wavelength of the pump light and fiber length and pulse duration on the SC, the simulations demonstrate that the MIR SC extending from 1.80 μm to 11.32 μm in the FM-PCF can be generated by pumping a 3.0-cm-long fiber at the central wavelength of 3.0 μm, the peak power of 120 W, and the pulse duration of 250 fs. The spectrum has better continuity and flatness, and the pump light source can be easily achieved.

Statements and Declarations

The authors declare that there are no conflicts of interest related to this article.

References

[1] STEINMEYER G, SKIBINA J S. Supercontinua：entering the mid-infrared[J]. Nature photonics, 2014, 8(11)：814-815.

[2] KALRA S, VYAS S, TIWARI M, et al. Multi-material photonic crystal fiber in MIR region for broadband supercontinuum generation[M]//Optical and wireless technologies. Berlin, Heidelberg：Springer, 2018, 472：199-209.

[3] WEI W, PENG X, DAI S, et al. Visible to mid-infrared supercontinuum generated in novel GeS_2-Ga_2S_3-CsI step-index fiber[J]. Journal of modern optics, 2019, 66(11)：1-7.

[4] ZHU Y, ZHENG Z, GE X, et al. High-power, ultra-broadband supercontinuum source based upon 1/1.5 m dual-band pumping[J]. Chinese optics letters, 2021, 19(4)：041403-1-041403-6.

[5] SAINI T S, KUMAR A, SINHA R K. Broadband mid-infrared supercontinuum spectra spanning 2–15 μm using As_2Se_3 chalcogenide glass triangular-core graded index photonic crystal fiber[J]. Journal of light wave technology, 2015, 33(18)：3914-3920.

[6] CHENG T, NAGASAKA K, TUAN T H, et al. Mid-infrared supercontinuum generation spanning 2.0 to 15.1μm in a chalcogenide step-index fiber[J]. Optics letters, 2016, 41(9)：2117-2120.

[7] WU B, ZHAO Z, WANG X, et al. Mid-infrared supercontinuum generation in a suspended-core tellurium-based chalcogenide fiber[J]. Optical materials express, 2018, 8(5)：1341-1348.

[8] GAO W, AMRAOUI M E, LIAO M, et al. Mid-infrared supercontinuum generation in a suspended-core As_2S_3 chalcogenide microstructured optical fiber[J]. Optics

express, 2013, 21(8)：9573-9583.

[9]   SHA B, SS A, MF A. Ultra-high birefringent, highly non-linear $Ge_{20}Sb_{15}Se_{65}$ chalcogenide glass photonic crystal fiber with zero dispersion wavelength for mid-infrared applications[J]. Optik, 2020, 225：1-27.

[10]   IRNIS K, OLE B. Multimode supercontinuum generation in chalcogenide glass fibres[J]. Optics express, 2016, 24(3)：2513-2526.

[11]   KHALIFA A B, SALEM A B, CHERIF R. Mid-infrared supercontinuum generation in multimode As_2Se_3 chalcogenide photonic crystal fiber[J]. Applied optics, 2017, 56(15)：4319-4324.

[12]   SWIDERSKI J, MICHALSKA M, MAZE G. Mid-IR supercontinuum generation in a ZBLAN fiber pumped by a gain-switched mode-locked Tm-doped fiber laser and amplifier system[J]. Optics express, 2013, 21(7)：7851-7857.

[13]   QIN G, XIN Y, KITO C, et al. Ultra-broadband supercontinuum generation from ultraviolet to 6.28 μm in a fluoride fiber[J]. Applied physics letters, 2009, 95(16)：584-588.

[14]   KUBAT I, PETERSEN C R, MØLLER U V, et al. Thulium pumped mid-infrared 0.9-9μm supercontinuum generation in concatenated fluoride and chalcogenide glass fibers[J]. Optics express, 2014, 22(4)：3959-3967.

[15]   SAFAEI A, BOLORIZADEH M A. Quantum mechanical treatment of the third order nonlinear term in NLS equation and the supercontinuum generation[C]//Photonic Fiber and Crystal Devices：Advances in Materials and Innovations in Device Applications X, August 28-September 1, 2016, San Diego, California, USA. Washington：SPIE, 2016：995803.

[16]   CHAITANYA A, SINGH S T, AJEET K, et al. Ultra broad-band mid-IR supercontinuum generation in $Ge_{11.5}As_{24}Se_{64.5}$ based chalcogenide graded-index photonic crystal fiber：design and analysis[J]. Applied optics, 2016, 55(36)：10138-10145.

[17]   FRANCESCO P, PETER H. Description of ultrashort pulse propagation in multimode optical fibers[J]. Journal of the optical society of America B, 2008, 25(10)：1645-1654.

[18]   FANG Y T, LIANG Z C. Unusual transmission through usual one-dimensional photonic crystal in the presence of evanescent wave[J]. Optics communications, 2010, 283(10)：2102-2108.